Supplemental figures and methods

Therapeutic Targeting of GCB- and ABC-DLBCLs by Rationally Designed BCL6 Inhibitors

Mariano G Cardenas[1], Wenbo Yu[2#], Wendy Beguelin[1], Matthew R Teater[1], Huimin Geng[1, 3], Rebecca L. Goldstein[1], Erin Oswald[1], Katerina Hatzi[1], Shao-Ning Yang[1], Joanna Cohen[1], Rita Shaknovich[1], Kenno Vanommeslaeghe[2, 7], Huimin Cheng[2], Dongdong Liang[2], Hyo Je Cho[4], Joshua Abbott[4], Wayne Tam[5], Wei Du[6], John P. Leonard[1], Olivier Elemento[6], Leandro Cerchietti[1*], Tomasz Cierpicki[4*], Fengtian Xue[2*], Alexander D. MacKerell, Jr.[2*], Ari M. Melnick[1*].

[1]Weill Cornell Medical College, Department of Hematology/Oncology, New York, NY. [2]Computer-Aided Drug Design Center, University of Maryland, School of Pharmacy, Department of Pharmaceutical Sciences, Baltimore, MD. [3]University of California San Francisco, Department of Laboratory Medicine, San Francisco, CA, USA. [4]University of Michigan, Department of Pathology, Ann Arbor, MI. [5]Department of Pathology and Laboratory Medicine, Weill Cornell Medical College, NY, USA. [6]Department of Physiology and Biophysics, Weill Cornell Medical College, NY, USA. [7]Department of Analytical Chemistry and Pharmaceutical Technology (FABI), Center for Pharmaceutical Research (CePhaR), Vrije Universiteit Brussel (VUB), Laarbeeklaan 103, B-1090 Brussels, Belgium. [#]Considered co-first author. [*]Corresponding authors.

A

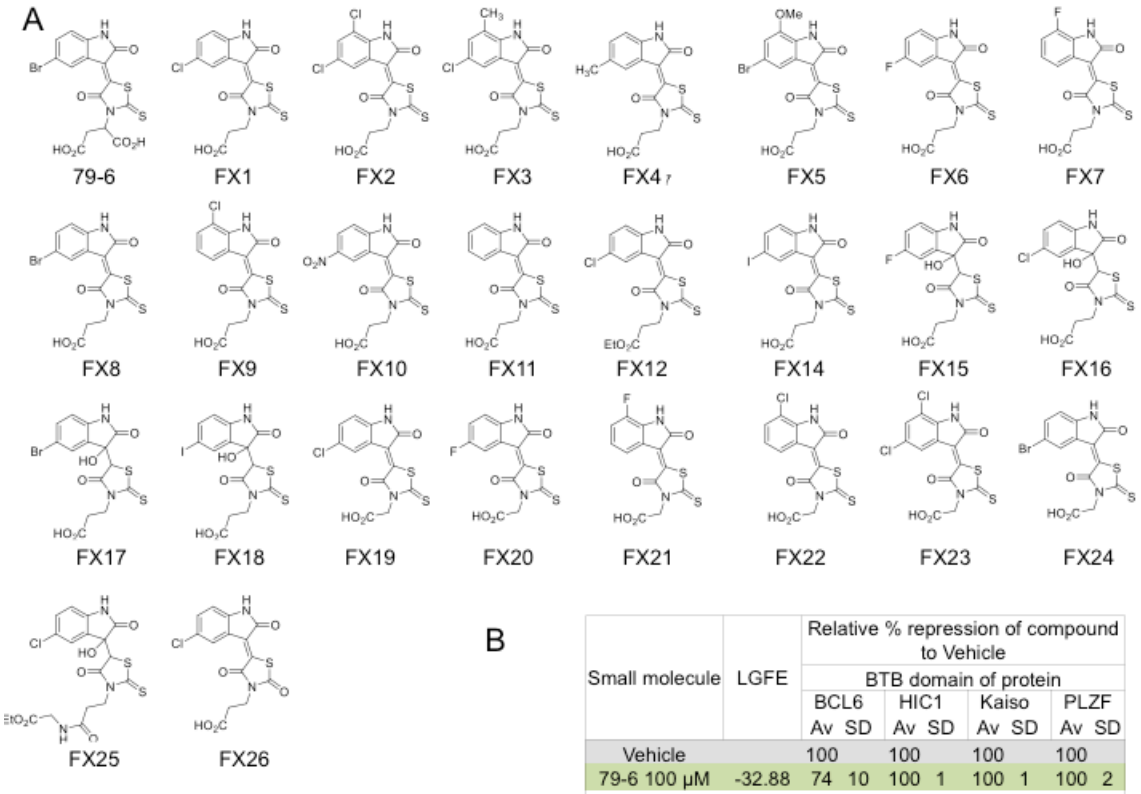

B

Small molecule	LGFE	Relative % repression of compound to Vehicle							
		BTB domain of protein							
		BCL6		HIC1		Kaiso		PLZF	
		Av	SD	Av	SD	Av	SD	Av	SD
Vehicle		100		100		100		100	
79-6 100 µM	-32.88	74	10	100	1	100	1	100	2
FX1 50 µM	-37.06	41	8	88	15	91	4	100	5
FX5 50 µM	-30.97	59	9	97	5	103	8	100	6
FX12 50 µM	-36.57	60	7	99	8	95	17	100	2
FX10 50 µM	-34.06	61	4	92	9	82	13	100	7
FX9 50 µM	-31.43	62	6	88	12	87	7	100	6
FX4 50 µM	-38.36	65	11	98	3	93	5	100	5
FX7 50 µM	-31.78	66	8	89	15	90	9	100	4
FX6 50 µM	-33.58	66	9	94	9	93	9	100	6
FX14 50 µM	-36.38	67	7	99	5	96	22	100	4
FX8 50 µM	-36.38	73	9	94	13	109	9	120	3
FX3 50 µM	-35.03	73	4	90	17	101	8	100	3
FX2 50 µM	-31.90	74	6	88	17	85	1	100	5
FX11 50 µM	-34.27	79	7	89	9	101	15	100	6
FX18 50 µM	-28.81	62	7	81	7	89	9	100	3
FX17 50 µM	-28.69	64	3	90	10	88	12	100	2
FX15 50 µM	-24.86	93	4	91	13	100	0	109	5
FX16 50 µM	-28.95	96	13	80	14	96	6	116	2
FX23 50 µM	-31.38	80	1	99	9	95	13	117	3
FX20 50 µM	-33.15	92	6	92	11	97	4	100	9
FX24 50 µM	-35.05	94	5	101	1	102	3	99	9
FX19 50 µM	-30.58	94	6	93	11	103	4	104	1
FX21 50 µM	-30.54	94	6	102	3	102	3	97	8
FX22 50 µM	-31.39	96	6	96	6	104	6	100	8
FX25 50 µM	-35.17	89	10	74	6	105	7	73	7
FX26 50 µM	-35.14	90	14	100	2	96	6	113	7

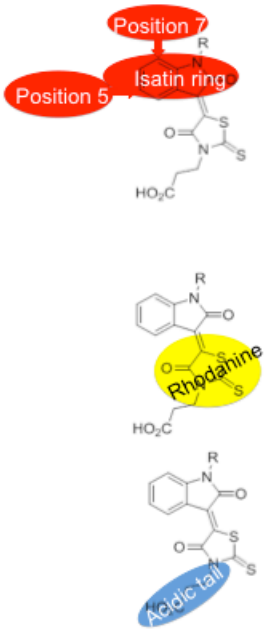

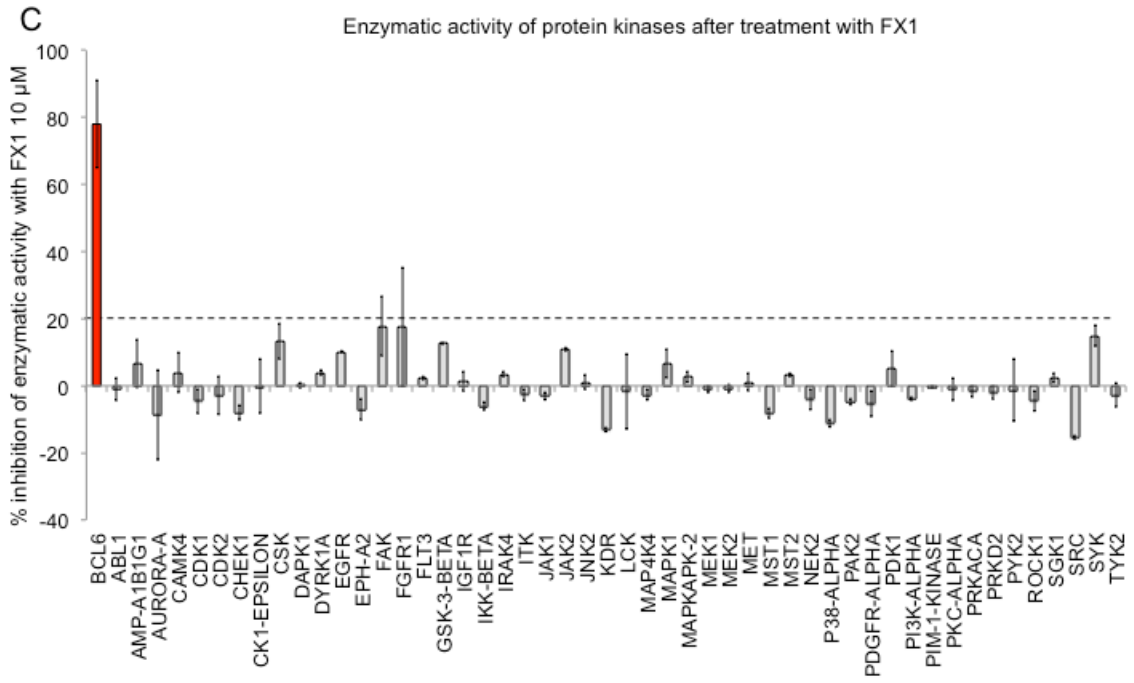

Supplemental Figure 1. FX1 is a specific and selective BCL6 inhibitor (**A**) Compounds chemical structures, with changes at different positions as represented in (B), were synthesized and purified for experimental assay together with 79-6. (**B**) Compounds were subjected to quantitative ranking using Monte Carlo (MC)-SILCS docking to the BCL6-BTB to calculate the ligand grid free energy (LGFE), which is an estimate of the binding affinity of a compound. Reporter assays were performed to test the activity of compounds with different BTB-related proteins (BCL6, HIC1, Kaiso, PLZF). The values show the percentage of repression of the GAL4-DBD-BTB fusion protein relative to GAL4-DBD alone and vehicle (which is set as 100%). Compounds were tested at 50 or 100 µM. The table is ordered according to the BCL6-BTB repression inhibition activity and shows mean ± SD of three independent experiments with compounds tested in quadruplicate. (**C**) Biochemical enzymatic activity of different kinases after treatment with 10 µM of FX1. Bars represent the percentage of inhibition and are the average of two independent measurements. The y-axis represents the percentage of kinase activity inhibition when comparing treatment with 10 µM of FX1 to the vehicle treated ones.

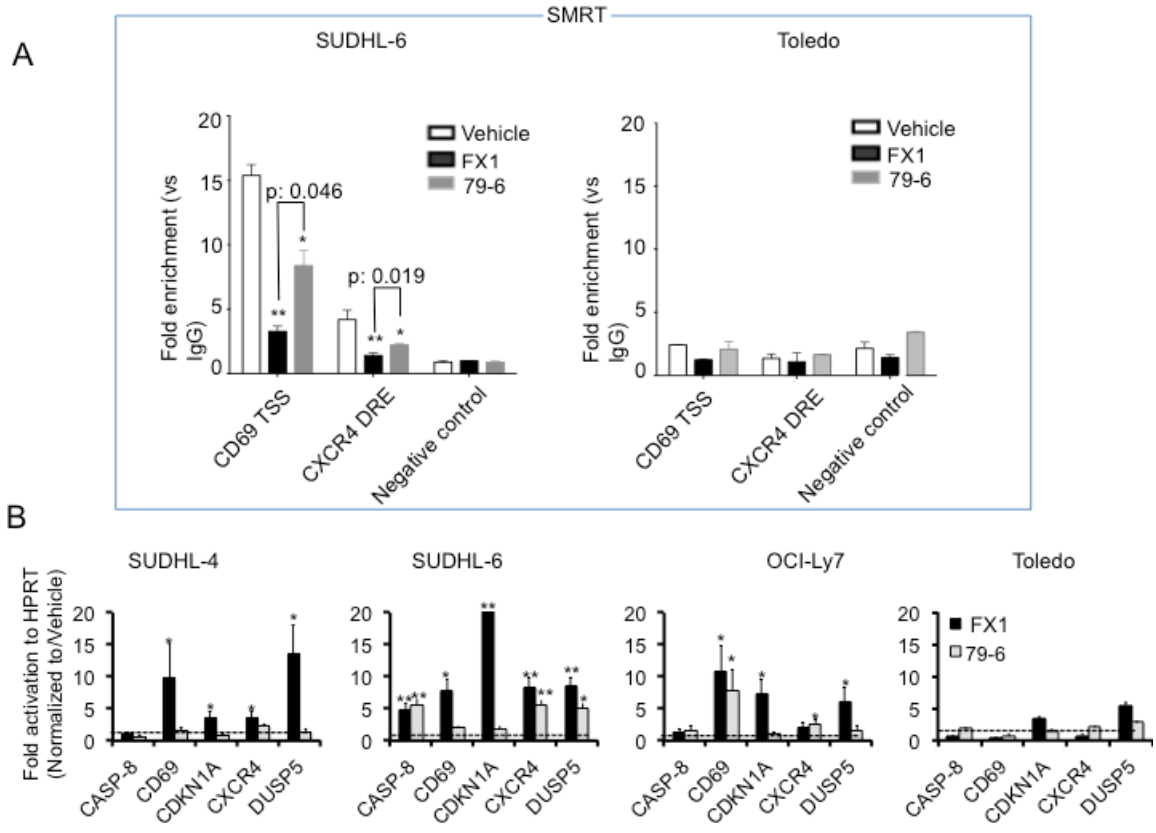

Supplemental Figure 2. FX1 is a better and more potent BCL6 inhibitor than 79-6 (**A**) QChIP was performed in SUDHL-6 and Toledo cells exposed to vehicle (white bars), 50 μM FX1 (black bars), or 79-6 (grey bars). Antibodies for SMRT or IgG control were used to enrich for known BCL6 binding sites in the CD69, CXCR4 and DUSP5 loci, or a negative control region. The y-axis represents fold enrichment of binding vs. input, as compared to IgG control, and represent mean ± SD of three independent experiments (t-test). (**B**) QPCR was performed in SUDHL-4, SUDHL6, OCI-Ly7, and Toledo cells after exposure to 50 μM FX1 (black bars), 79-6 (grey bars) or vehicle (horizontal stripped line) to measure abundance of the BCL6 target genes CASP8, CD69, CXCR4, CDKN1A and DUSP5. The y-axis shows fold enrichment vs. HPRT mRNA based on the $\Delta\Delta^{Ct}$ values. Fold activation was calculated by dividing $\Delta\Delta^{Ct}$ values of the treated ones to the vehicle. Bar graphs in A and B show average ± SD of three independent experiments (* p <0.05 ** p <0.005, t-test).

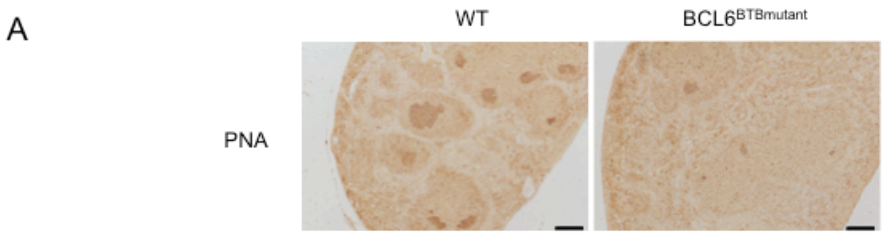

Supplemental Figure 3. FX1 phenocopies the BCL6 mutant phenotype. (**A**) Immunohistochemistry and staining with peanut agglutinin (PNA) was performed on spleen sections from $BCL6^{BTBMUT}$ mice 10 days after immunization with SRBCs. Scale bars represent 200 μm.

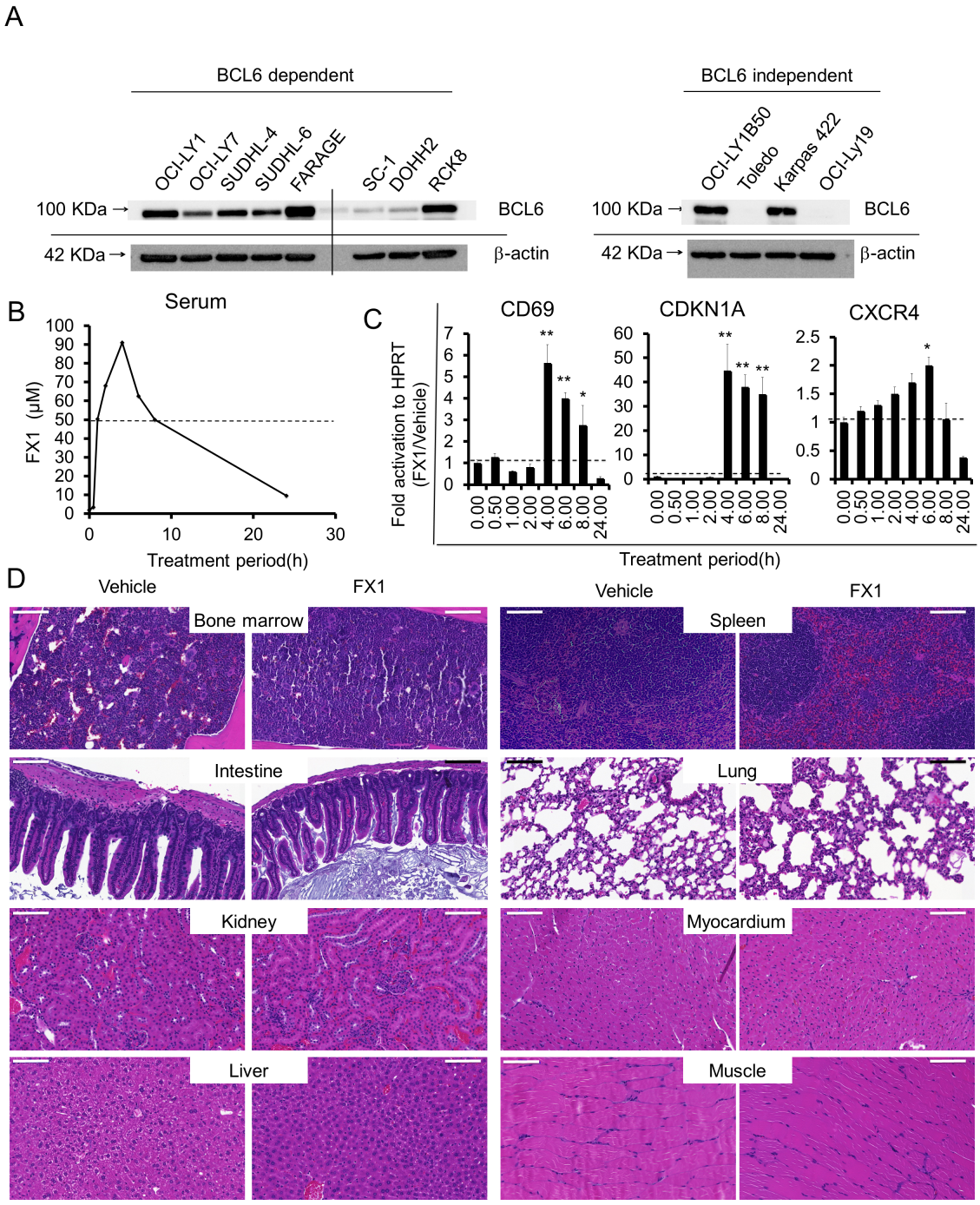
A
BCL6 dependent
BCL6 independent
OCI-LY1
OCI-LY7
SUDHL-4
SUDHL-6
FARAGE
SC-1
DOHH2
RCK8
OCI-LY1B50
Toledo
Karpas 422
OCI-Ly19
100 KDa →
BCL6
42 KDa →
β-actin
B
Serum
FX1 (μM)
Treatment period(h)
C
CD69
CDKN1A
CXCR4
Fold activation to HPRT (FX1/Vehicle)
Treatment period(h)
D
Vehicle
FX1
Bone marrow
Spleen
Intestine
Lung
Kidney
Myocardium
Liver
Muscle

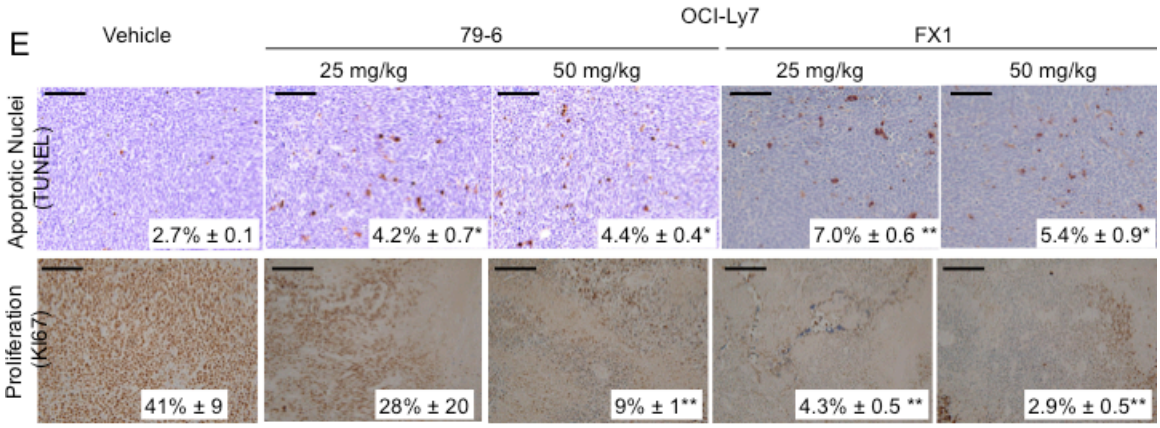
E
Vehicle
OCI-Ly7
79-6
FX1
25 mg/kg
50 mg/kg
25 mg/kg
50 mg/kg
Apoptotic Nuclei (TUNEL)
2.7% ± 0.1
4.2% ± 0.7*
4.4% ± 0.4*
7.0% ± 0.6 **
5.4% ± 0.9*
Proliferation (Ki67)
41% ± 9
28% ± 20
9% ± 1**
4.3% ± 0.5 **
2.9% ± 0.5**

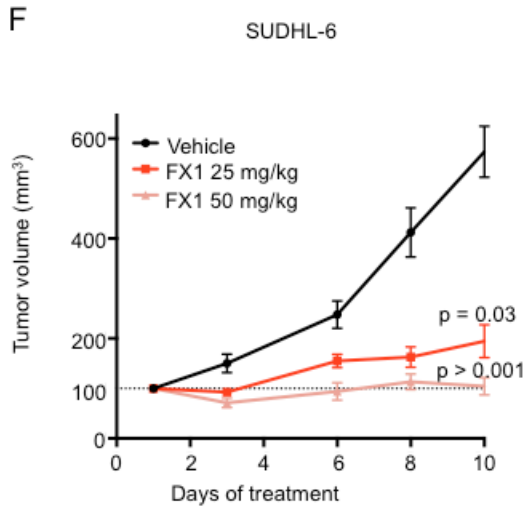
F
SUDHL-6
Tumor volume (mm3)
Vehicle
FX1 25 mg/kg
FX1 50 mg/kg
p = 0.03
p > 0.001
Days of treatment

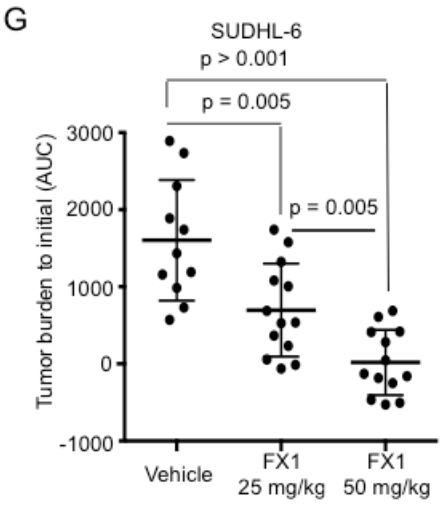
G
SUDHL-6
p > 0.001
p = 0.005
p = 0.005
Tumor burden to initial (AUC)
Vehicle
FX1 25 mg/kg
FX1 50 mg/kg

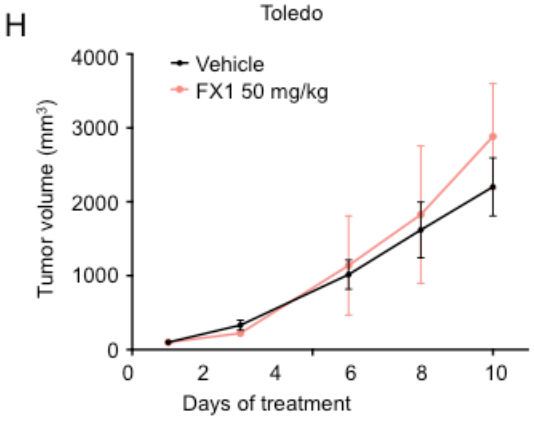
H
Toledo
Tumor volume (mm3)
Vehicle
FX1 50 mg/kg
Days of treatment

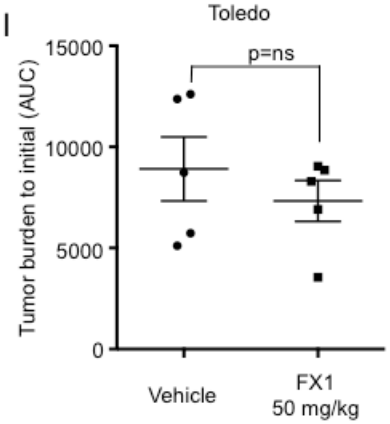
I
Toledo
p=ns
Tumor burden to initial (AUC)
Vehicle
FX1 50 mg/kg

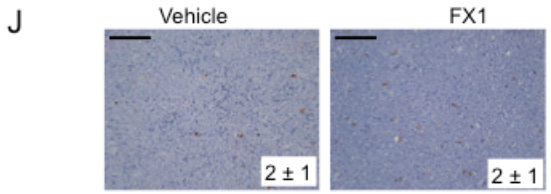

Supplemental Figure 4. FX1 displays favorable pharmacokinetics and is nontoxic to animals (**A**) BCL6 immunoblot was performed in BCL6-dependent and -independent cell lines. BCL6 and β-actin were run on the same lane of the gel but were noncontiguous and are separated by a dividing line. (**B**) Serum concentration of FX1 (μM, y-axis) was calculated after treating 1000 cm^3 SUDHL-6 tumor-bearing SCID mice with 50 mg/kg FX1 for different time points. FX1 serum concentration was determined by HPLC/MS (spotted line: average GI_{50} of sensitive cells lines). (**C**) QPCR was performed in pulverized tumors from the same mice as (**B**). The y-axis shows fold enrichment vs. HPRT mRNA based on the $\Delta\Delta^{CT}$ values (* $p < 0.05$ ** $p < 0.005$, t-test). (**D**) H&E staining of organ tissue sections from C57BL/6 mice treated with 100 mg/kg FX1 daily. (**E**) TUNEL and KI67 immunohistochemistry was performed in OCI-Ly7 xenografts. (n = 25, * $p < 0.05$ ** $p < 0.005$, t-test). Tumor volume of established SUDHL-6 (**F**) and Toledo (**H**) xenografts implanted in SCID mice were calculated following treatment with vehicle, 25 mg/kg of FX1, or 50 mg/kg of FX1 daily for 10 days (n=30, two-tailed Mann-Whitney unpaired test). The y-axis represent the tumor volume related to the initial (100 mm^3). (**G**) and (**I**) Tumor burden area under the curve from the same mice as in (**F**) and (**H**) were calculated between the initial tumor volume (dotted line) and the volume at day 10 (two-tailed Mann-Whitney unpaired test). The y-axis represents the area under the curve (AUC) to the initial volume. (**J**) TUNEL immunohistochemistry performed in Toledo xenografts from mice treated with 50 mg/kg FX1 or vehicle (n = 10, t-test). Measurements in (**F**), (**G**), (**H**), and (**I**) represent mean ± SD of 5 tumors. Scale bars in (**D**), (**E**) and (**J**) represent 100 μm.

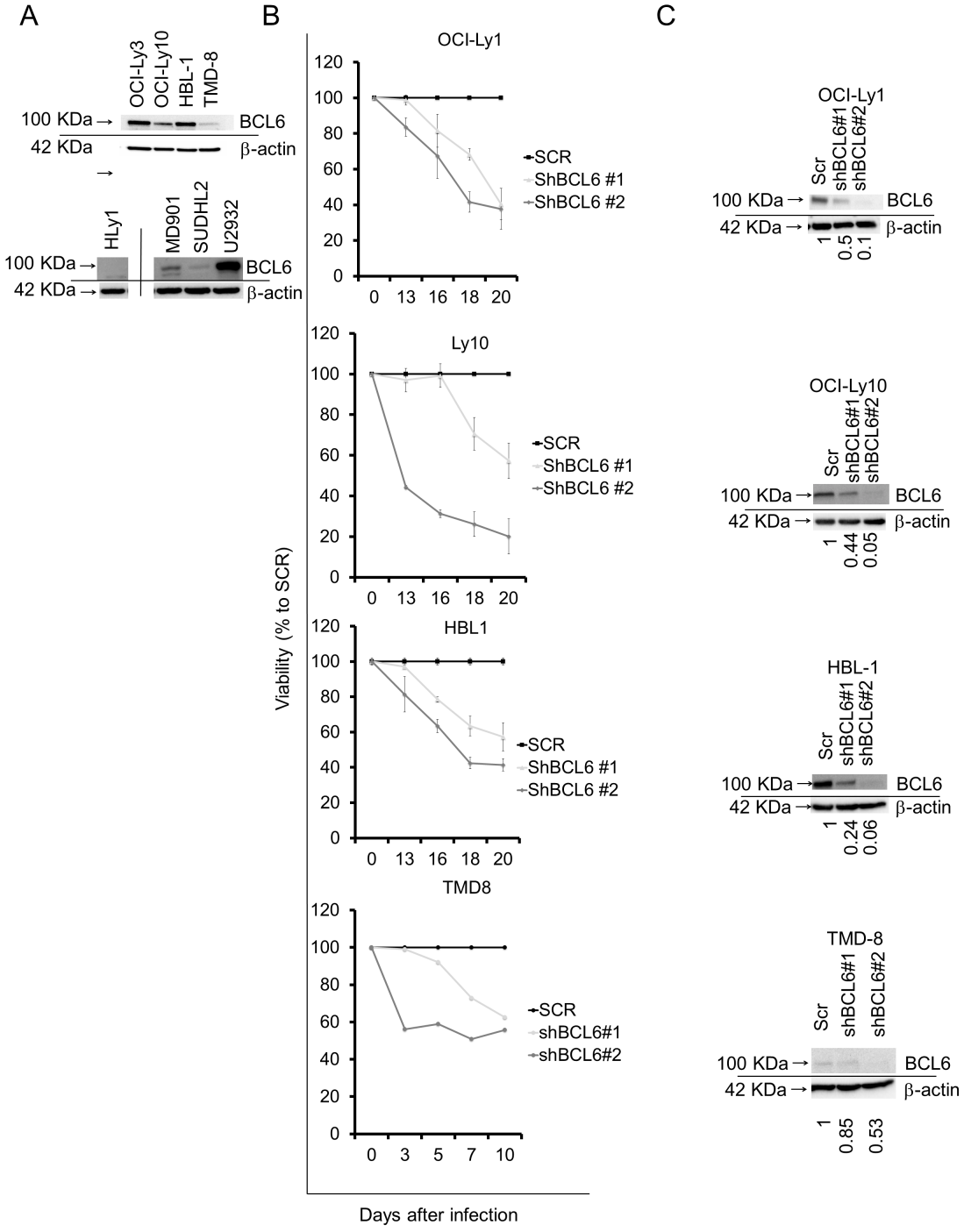
A
OCI-Ly3
OCI-Ly10
HBL-1
TMD-8
100 KDa →
BCL6
42 KDa
β-actin
HLy1
MD901
SUDHL2
U2932
100 KDa →
BCL6
42 KDa →
β-actin
B
OCI-Ly1
Ly10
HBL1
TMD8
Viability (% to SCR)
SCR
ShBCL6 #1
ShBCL6 #2
shBCL6#1
shBCL6#2
Days after infection
C
OCI-Ly1
Scr
shBCL6#1
shBCL6#2
100 KDa →
BCL6
42 KDa →
β-actin
1
0.5
0.1
OCI-Ly10
1
0.44
0.05
HBL-1
1
0.24
0.06
TMD-8
1
0.85
0.53

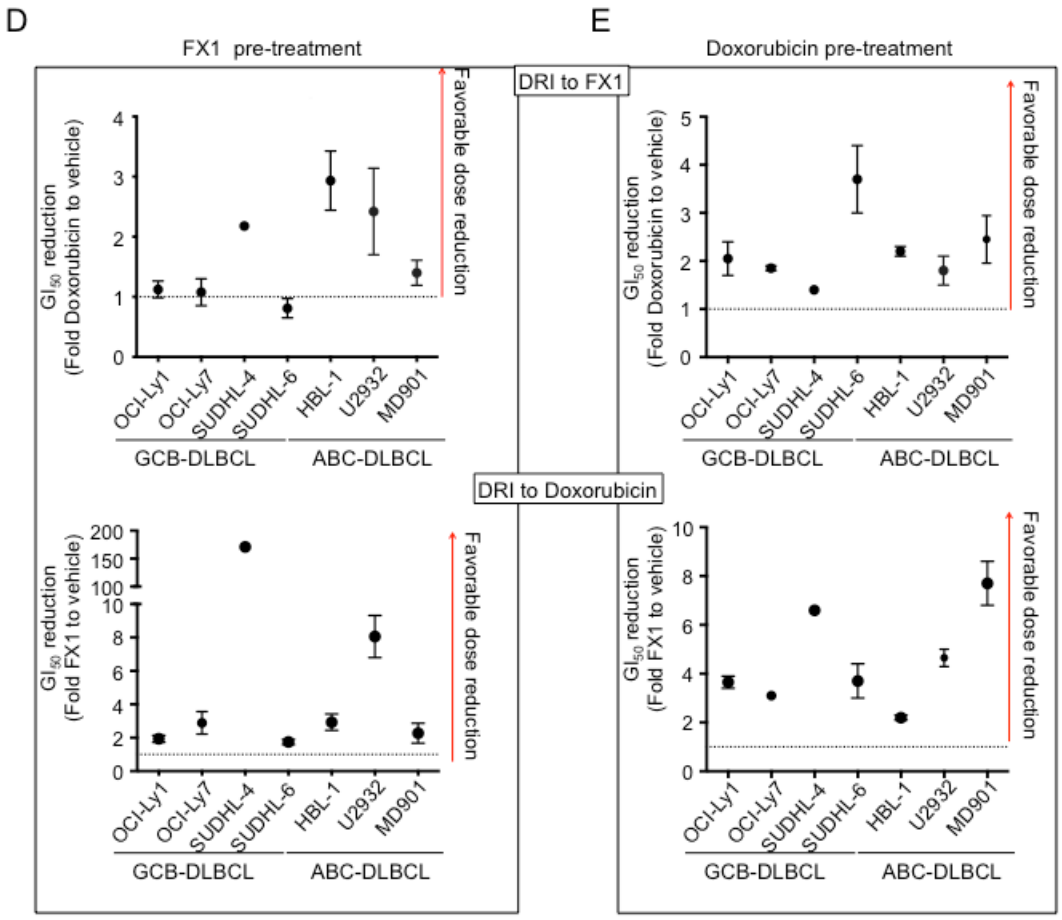

Supplemental Figure 5. ABC-DLBCLs are dependent on BCL6 for survival. (**A**) BCL6 immunoblot was performed in eight ABC-DLBCL cell lines (OCI-Ly3, OCI-Ly10, HBL-1, TMD8, Hly1, MD901, SUDHL2, U2932). BCL6 and β-actin were run on the same lane of the gel but were noncontiguous and are separated by a dividing line. (**B**) One GCB-DLBCL (OCI-Ly1) and three ABC-DLBCL (OCI-Ly10, HBL-1, TMD8) were transduced with GFP-tagged lentivirus expressing BCL6 shRNA #1 (light grey line), BCL6 shRNA #2 (dark grey line), or a non-targeted control shRNA (black line). Viability (represented as percentage to Scramble, SCR) was determined using flow cytometry after different timepoints of transduction and is plotted on the y-axis. Live cells were defined as GFP positive cells that were Annexin V/DAPI double negative. Data shows mean ± SEM of 2 biological replicates. (**C**) BCL6 immunoblot was performed in cells treated with the same lentivirus as in (**B**). The ratio of the amount of BCL6 to actin, relative to SCR, was quantified by densitometry (indicated by numbers below BCL6 immunoblots). Sequential administration and assessment of dose reduction index of FX1 followed by doxorubicin. BCL6 and β-actin were run on the same lane of the gel but were noncontiguous and are separated by a dividing line. (**D**) or doxorubicin followed by FX1 (**E**) was calculated in the indicated cell lines by the resazurin reduction. Cells were pre-treated with the first drug, followed by treatment with the second drug 24 hours later. Proliferation was analyzed 48 hours after treatment with the second drug based on resazurin reduction. DRI higher than 1 for doxorubicin (top) or FX1 (bottom) represents a favorable combination. Data shows mean ± SEM of 3 biological replicates

Supplemental methods

Computational Methods

The Site-Identification by Ligand Competitive Saturation (SILCS) method (1-4) was used to model the binding of the designed inhibitors with the BCL6 BTB domain. The crystal structure of the BCL6 BTB – SMRT peptide complex (PDB ID: 1R2B) (5), following removal of the SMRT peptide was used to initialize the molecular modeling study. The Reduce software was used to choose optimal Asn, Gln, and His side-chain orientations and determine the optimal protonation states of His residues (6).(6). The protein was immersed in a box of an aqueous solution containing eight small probe molecules at approximately 0.25 M each with water at ~55 M. The size of the simulation box was chosen so as to have the protein extrema separated from the edges by a minimum of 8 Å based on non-hydrogen atoms. The small molecules include benzene, propane, methanol, formamide, acetaldehyde, methylammonium and acetate, as previously used (3), along with imidazole. Ten such protein-small molecule aqueous systems were generated with each simulation system differing in the initial positions and orientations of the small molecules and water. The SILCS molecular dynamics (MD) simulations were performed using the GROMACS simulation program (7) with the CHARMM36 protein force field (7) with the CHARMM36 protein force field (8, 9), CHARMM general force field (CGenFF) (10), in conjunction with the CGenFF program (10), in conjunction with the CGenFF program (11, 12) and TIP3P water model (13) to describe the protein, small molecules and water, respectively. The ten simulations were each extended for 40 ns, yielding a total of 400 ns of simulation time. Details about SILCS simulation setups can be found in reference (3)

From the simulation, 3D probability distributions of selected atoms from the small probe molecules were constructed to form the FragMaps, yielding a total of ten different FragMaps. The FragMaps were converted to free energies, termed grid free energies

(GFE), by normalizing the distributions with respect to the distributions of the solutes in an aqueous solution in the absence of the proteins followed by Boltzmann transformation to yield the GFE values (3). In addition, as a substitute for the protein solvent accessible surface, “exclusion” maps were constructed by calculating the 3D probability distributions of all non-hydrogen atoms of the probe molecules and water together and identifying those voxels with zero occupancies, such that the exclusion map represents the protein surface as the region that is not sampled by water or probe molecules during the SILCS simulations The exclusion map represents regions forbidden to the probe molecules and water and may be considered as an alternate to more traditional representations of the protein surface. For quantitative analysis, these voxels were assigned a very high energetic penalty (1000 kcal/mol) while the remaining voxels were assigned energies associated with the specific FragMaps. The availability of the GFE FragMaps and the exclusion maps allows for quantitative estimates of binding affinities to be made referred to as ligand grid free energies (LGFE) (3). These are a simple summation of the GFE energy contribution of all the atoms in each ligand that are classified with respect to the FragMap types followed by normalization of the summed energies by the number of classified ligands atoms and subsequent multiplication by the total number of non-hydrogen atoms, yielding the final LGFE values. Note that the LGFE scores are not directly equivalent to experimental free energies due to the additive approximation of the LGFE scores (i.e. the individual atom-based GFEs are summed to yield the LGFE) and the lack of accounting for the energy cost of connecting the fragments that comprise the full compounds.

The BCL6 inhibitors were docked into the 79-6 binding site using FragMap-based Monte Carlo (MC) sampling (MC-SILCS)(3) from which the LGFE scores were also obtained. The each compound was initially aligned with 79-6 in its bound orientation. MC-SILCS on each compound was applied multiple times to ensure convergence. The

individual MC-SILCS runs involved a two-step protocol. For the first step, MC-SILCS was performed for 10000 steps under the normal MC mode where the compound was allowed to move relatively freely from the initial orientation to explore the surrounding binding pocket region. MC-SILCS, initiated from the most favorable LGFE-binding orientation from the first 10000 steps, was continued under a slow cooling MC mode where the temperature was decreased from room temperature to 0 K over 40000 steps thereby identifying the local minimum for which the LGFE score was obtained. 50 independent MC-SILCS runs were performed and a check made to determine if the three most favourable LGFE scores were within 0.5 kcal/mol of each other to assure convergence. If this requirement was not met the MC-SILCS runs were repeated until the LGFE difference between the top three most favourable binding orientations were within 0.5 kcal/mol. The lowest LGFE conformation was then chosen as the predicted binding mode for the compound for which the LGFE score was obtained

Synthesis and Characterization of New Compounds

General Method A: Knoevenagel Condensation. To a mixture of chloroisatin (1.0 mmol), 3-(4-oxo-2-thioxothiazolidin-3-yl)propanoic acid (205 mg, 1.0 mmol) and NaOAc (820 mg, 10.0 mmol) was added acetic acid (5.0 mL). The reaction was allowed to stir at 105 °C for 30 min - 12 h, then cooled to room temperature. To the reaction was added water (15 mL). The resulting mixture was sonicated to give an orange-red slurry. After filtration, the solid was washed with water (75 mL) and dried under high vacuum to yield the corresponding product as a red fine powder (71-92%):

(*Z*)-3-(5-(5-Chloro-2-oxoindolin-3-ylidene)-4-oxo-2-thioxothiazolidin-3-yl)propanoic acid (**FX1**). This compound was synthesized using general method A (89%): ^{1}H NMR (400 MHz, DMSO-d_6) δ 2.60-2.70 (t, *J* = 7.6 Hz, 2H), 4.20-4.30 (t, *J* =8.0 Hz, 2H), 6.90-7.00 (d, *J* = 8.0 Hz, 1H), 7.40-7.50 (dd, *J* = 2.0, 8.4 Hz, 1H), 8.80-8.81 (d, *J* = 2.0 Hz,

1H), 11.41 (s, 1H), 12.40-12.70 (br s, 1H); ^{13}C NMR (100 MHz, DMSO-d_6) δ 30.8, 112.2, 121.0, 123.8, 126.0, 127.0, 132.3, 132.8, 143.3, 166.6, 167.7, 171.7, 197.1; LC-TOF ($M+H^+$) calcd for $C_{14}H_{10}ClN_2O_4S_2$ 368.9771, found 368.9787.

(*Z*)-3-(5-(5,7-Dichloro-2-oxoindolin-3-ylidene)-4-oxo-2-thioxothiazolidin-3-yl)propanoic acid (**1093**). This compound was synthesized using general method A (80%): ^{1}H NMR (400 MHz, DMSO-d_6) δ 2.60-2.70 (t, *J* = 7.6 Hz, 2H), 4.25-4.35 (t, *J* =8.0 Hz, 2H), 7.10-7.15 (d, *J* = 1.6 Hz, 1H), 8.77-8.80 (d, *J* = 1.6 Hz, 1H), 11.86 (s, 1H), 12.40-12.70 (br s, 1H); ^{13}C NMR (100 MHz, DMSO-d_6) δ 30.8, 115.6, 122.2, 123.0, 125.6, 126.3, 131.3, 134.9, 140.9, 166.6, 167.8, 171.7, 196.7; LC-TOF ($M+H^+$) calcd for $C_{14}H_9Cl_2N_2O_4S_2$ 402.9381, found 402.9383.

(*Z*)-3-(5-(5-Chloro-7-methyl-2-oxoindolin-3-ylidene)-4-oxo-2-thioxothiazolidin-3-yl)propanoic acid (**1095**). This compound was synthesized using general method A (83%): ^{1}H NMR (400 MHz, DMSO-d_6) δ 2.23, (s, 3H), 2.60-2.70 (t, *J* = 7.6 Hz, 2H), 4.20-4.30 (t, *J* =8.0 Hz, 2H), 7.35 (s, 1H), 8.67 (s, 1H), 11.43 (s, 1H), 12.40-12.70 (br s, 1H); ^{13}C NMR (100 MHz, DMSO-d_6) δ 16.6, 31.2, 121.0, 122.6, 124.8, 126.3, 133.7, 142.5, 167.0, 168.6, 172.2, 197.6; LC-TOF ($M+H^+$) calcd for $C_{15}H_{12}ClN_2O_4S_2$ 382.9927, found 382.9927.

(*Z*)-3-(5-(5-Methyl-2-oxoindolin-3-ylidene)-4-oxo-2-thioxothiazolidin-3-yl)propanoic acid (**1097**). This compound was synthesized using general method A (90%): ^{1}H NMR (400 MHz, DMSO-d_6) δ 2.32, (s, 3H), 2.60-2.70 (t, *J* = 7.6 Hz, 2H), 4.20-4.30 (t, *J* =8.0 Hz, 2H), 6.80-6.90 (d, *J* = 8.0 Hz, 1H), 7.20-7.25 (d, *J* = 8.0 Hz, 1H), 8.64 (s, 1H), 11.16 (s, 1H), 12.40-12.70 (br s, 1H); ^{13}C NMR (100 MHz, DMSO-d_6) δ 20.8, 30.7, 110.4, 119.8, 125.4, 128.1, 130.3, 130.8, 133.6, 142.4, 166.4, 167.9, 171.7, 197.4; LC-TOF ($M+H^+$) calcd for $C_{15}H_{13}N_2O_4S_2$ 349.0317, found 349.0316.

(*Z*)-3-(5-(5-Bromo-7-methoxy-2-oxoindolin-3-ylidene)-4-oxo-2-thioxothiazolidin-3-yl)propanoic acid (**1113**). This compound was synthesized using general method A

(85%): ^{1}H NMR (400 MHz, DMSO-d_6) δ 2.60-2.70 (t, J = 7.6 Hz, 2H), 4.20-4.26 (t, J =8.0 Hz, 2H), 4.32 (s, 3H), 7.36 (s, 1H), 8.60 (s, 1H), 11.51 (s, 1H), 12.30-12.70 (br s, 1H); ^{13}C NMR (100 MHz, DMSO-d_6) δ 30.8, 111.6, 114.1, 114.4, 119.3, 119.6, 124.5, 132.7, 141.1, 156.4, 158.7, 166.7, 168.0, 171.8, 197.2; LC-TOF ($M+H^+$) calcd for $C_{15}H_{12}BrN_2O_5S_2$ 442.9371, found 442.9373.

(*Z*)-3-(5-(5-Fluoro-2-oxoindolin-3-ylidene)-4-oxo-2-thioxothiazolidin-3-yl)propanoic acid (**1115**). This compound was synthesized using general method A (86%): ^{1}H NMR (400 MHz, DMSO-d_6) δ 2.60-2.70 (t, J = 7.6 Hz, 2H), 4.20-4.26 (t, J =8.0 Hz, 2H), 6.90-7.00 (dd, J = 4.0, 8.0 Hz, 1H), 7.20-7.30 (m, 1H), 8.50-8.60 (d, J = 8.0 Hz, 1H), 11.31 (s, 1H), 12.30-12.70 (br s, 1H); ^{13}C NMR (100 MHz, DMSO-d_6) δ 30.8, 111.6, 114.1, 114.4, 119.3, 119.6, 124.5, 132.7, 141.1, 156.4, 158.7, 166.7, 168.0, 171.8, 197.2; LC-TOF ($M+H^+$) calcd for $C_{14}H_{10}FN_2O_4S_2$ 353.0066, found 353.0060.

(*Z*)-3-(5-(7-Fluoro-2-oxoindolin-3-ylidene)-4-oxo-2-thioxothiazolidin-3-yl)propanoic acid (**1117**). This compound was synthesized using general method A (92%): ^{1}H NMR (400 MHz, DMSO-d_6) δ 2.60-2.70 (t, J = 7.2 Hz, 2H), 4.20-4.26 (t, J =8.0 Hz, 2H), 7.10-7.20 (m, 1H), 7.36-7.42 (dd, J = 8.8, 9.2 Hz, 1H), 11.83 (s, 1H), 12.54 (br s, 1H); ^{13}C NMR (100 MHz, DMSO-d_6) δ 30.8, 119.5, 119.7, 122.5, 122.6, 122.8, 122.9, 123.9, 124.2, 124.3, 131.5, 131.7, 132.9, 145.5, 147.9, 166.5, 167.9, 171.8, 197.2; LC-TOF ($M+H^+$) calcd for $C_{14}H_{10}FN_2O_4S_2$ 353.0066, found 353.0059.

(*Z*)-3-(5-(5-Bromo-2-oxoindolin-3-ylidene)-4-oxo-2-thioxothiazolidin-3-yl)propanoic acid (**1165**). This compound was synthesized using general method A (85%): ^{1}H NMR (400 MHz, DMSO-d_6) δ 2.46-2.57 (t, J = 7.6 Hz, 2H), 4.20-4.26 (t, J =7.6 Hz, 2H), 6.80-6.90 (d, J = 7.6 Hz, 1H), 7.52-7.57 (d, J = 8.0 Hz, 1H), 8.93 (s, 1H), 11.39 (s, 1H), 12.30-12.70 (br s, 1H); ^{13}C NMR (100 MHz, DMSO-d_6) δ 30.8, 112.7, 113.7, 121.6, 123.7, 129.8, 135.1, 143.7, 166.7, 167.7, 171.7, 197.1; LC-TOF ($M+H^+$) calcd for $C_{14}H_{10}BrN_2O_4S_2$ 412.9265, found 412.9279.

(*Z*)-3-(5-(7-Chloro-2-oxoindolin-3-ylidene)-4-oxo-2-thioxothiazolidin-3-yl)propanoic acid (**1167**). This compound was synthesized using general method A (90%): ^{1}H NMR (400 MHz, DMSO-d_6) δ 2.60-2.70 (t, *J* = 8.0 Hz, 2H), 4.20-4.30 (t, *J* =7.6 Hz, 2H), 7.10-7.15 (t, *J* = 8.0 Hz, 1H), 7.50-7.55 (d, *J* = 7.6 Hz, 1H), 8.70-8.80 (d, *J* = 8.0 Hz, 1H), 11.71 (s, 1H), 12.40-12.80 (br s, 1H); ^{13}C NMR (100 MHz, DMSO-d_6) δ 30.8, 114.9, 121.5, 123.3, 124.3, 126.3, 132.4, 133.0, 141.9, 166.5, 168.0, 171.8, 197.1; LC-TOF ($M+H^+$) calcd for $C_{14}H_{10}ClN_2O_4S_2$ 368.9771, found 368.9791.

(*Z*)-3-(5-(5-Nitro-2-oxoindolin-3-ylidene)-4-oxo-2-thioxothiazolidin-3-yl)propanoic acid (**1169**). This compound was synthesized using general method A (86%): ^{1}H NMR (400 MHz, DMSO-d_6) δ 2.60-2.70 (m, 2H), 4.20-4.30 (m, 2H), 7.00-7.10 (d, *J* = 8.4 Hz, 1H), 8.20-8.30 (dd, *J* = 1.6, 8.4 Hz, 1H), 9.50-9.60 (d, *J* = 1.6 Hz, 1H), 11.92 (s, 1H), 13.00-14.00 (br s, 1H); ^{13}C NMR (100 MHz, DMSO-d_6) δ 31.1, 111.4, 120.2, 123.2, 129.0, 135.0, 142.7, 150.1, 167.1, 168.8, 172.1, 197.0; LC-TOF ($M+H^+$) calcd for $C_{14}H_{10}N_3O_6S_2$ 380.0011, found 380.0011.

(*Z*)-3-(4-Oxo-5-(2-oxoindolin-3-ylidene)-2-thioxothiazolidin-3-yl)propanoic acid (**2001**). This compound was synthesized using general method A (75%): ^{1}H NMR (400 MHz, DMSO-d_6) δ 1.12-1.16 (t, *J* = 4.0 Hz, 3H), 2.60-2.75 (t, *J* = 8.0 Hz, 2H), 4.00-4.10 (m, 2H), 4.20-4.30 (m, 2H), 6.90-6.95 (d, *J* = 8.0 Hz, 1H), 7.40-7.50 (dd, *J* = 2.0, 8.0 Hz, 1H), 8.75-8.80 (d, *J* = 2.0 Hz, 1H), 11.37 (s, 1H), 13.00-14.00 (br s, 1H); ^{13}C NMR (100 MHz, DMSO-d_6) δ 13.4, 30.3, 59.9, 111.7, 120.5, 123.4, 125.5, 131.8, 132.2, 142.9, 166.1, 167.2, 169.6, 196.6; LC-TOF ($M+H^+$) calcd for $C_{14}H_{11}N_2O_4S_2$ 335.0160, found 335.0166.

(*Z*)-Ethyl-3-(5-(5-chloro-2-oxoindolin-3-ylidene)-4-oxo-2-thioxothiazolidin-3-yl)propanoate (**2003**). This compound was synthesized using general method A (74%): ^{1}H NMR (400 MHz, DMSO-d_6) δ 1.12-1.16 (t, *J* = 4.0 Hz, 3H), 2.60-2.75 (t, *J* = 8.0 Hz, 2H), 4.00-4.10 (m, 2H), 4.20-4.30 (m, 2H), 6.90-6.95 (d, *J* = 8.0 Hz, 1H), 7.40-7.50 (dd, *J*

= 2.0, 8.0 Hz, 1H), 8.75-8.80 (d, *J* = 2.0 Hz, 1H), 11.37 (s, 1H), 13.00-14.00 (br s, 1H); ^{13}C NMR (100 MHz, DMSO-d_6) δ 13.4, 30.3, 59.9, 111.7, 120.5, 123.4, 125.5, 131.8, 132.2, 142.9, 166.1, 167.2, 169.6, 196.6; LC-TOF ($M+H^+$) calcd for $C_{16}H_{14}ClN_2O_4S_2$ 397.0084, found 397.0081.

(*Z*)-3-(5-(5-Iodo-2-oxoindolin-3-ylidene)-4-oxo-2-thioxothiazolidin-3-yl)propanoic acid (**2005**). This compound was synthesized using general method A (88%): ^{1}H NMR (400 MHz, DMSO-d_6) δ 2.60-2.70 (t, *J* = 8.0 Hz, 2H), 4.20-4.30 (m, 2H), 6.80-6.85 (d, *J* = 8.0 Hz, 1H), 7.70-7.75 (d, *J* = 8.0 Hz, 1H), 9.12 (s, 1H), 11.40 (s, 1H), 13.00-14.00 (br s, 1H); ^{13}C NMR (100 MHz, DMSO-d_6) δ 30.8, 85.2, 113.1, 122.0, 123.6, 132.6, 135.5, 140.9, 144.1, 166.7, 167.5, 171.8, 197.2; LC-TOF ($M+H^+$) calcd for $C_{10}H_{16}N_2O_4$ 460.9127, found 460.9206.

(*Z*)-2-(5-(5-Chloro-2-oxoindolin-3-ylidene)-4-oxo-2-thioxothiazolidin-3-yl)acetic acid (**2031**). This compound was synthesized using general method A (85%): ^{1}H NMR (400 MHz, DMSO-d_6) δ 4.76 (s, 2H), 6.90-6.96 (d, *J* = 8.8 Hz, 1H), 7.40-7.45 (dd, *J* = 1.6, 8.0 Hz, 1H), 8.70 (s, 1H), 11.39 (s, 1H), 13.00-14.00 (br s, 1H); ^{13}C NMR (100 MHz, DMSO-d_6) δ 45.2, 112.7, 121.4, 125.5, 126.5, 127.4, 131.7, 133.1, 144.1, 166.8, 167.6, 167.6, 168.0, 197.4; LC-TOF ($M+H^+$) calcd for $C_{13}H_8ClN_2O_4S_2$ 354.9614, found 354.9618.

(*Z*)-2-(5-(5-Fluoro-2-oxoindolin-3-ylidene)-4-oxo-2-thioxothiazolidin-3-yl)acetic acid (**2033**). This compound was synthesized using general method A (85%): ^{1}H NMR (400 MHz, DMSO-d_6) δ 4.76 (s, 2H), 6.90-7.00 (dd, *J* = 4.0, 8.0 Hz, 1H), 7.26-7.30 (m, 1H), 8.40-8.50 (dd, *J* = 2.8, 10.0 Hz, 1H), 11.29 (s, 1H), 13.00-14.00 (br s, 1H); ^{13}C NMR (100 MHz, DMSO-d_6) δ 44.9, 1118, 114.3, 114.5, 119.8, 120.1, 125.8, 131.2, 141.5, 156.5, 158.8, 166.5, 167.3, 168.0, 197.2; LC-TOF ($M+H^+$) calcd for $C_{13}H_8FN_2O_4S_2$ 338.9910, found 338.9908.

(*Z*)-2-(5-(7-Fluoro-2-oxoindolin-3-ylidene)-4-oxo-2-thioxothiazolidin-3-yl)acetic acid (**2035**). This compound was synthesized using general method A (72%): ^{1}H NMR (400

MHz, DMSO-d_6) δ 4.78 (s, 2H), 7.00-7.15 (m, 1H), 7.36-7.41 (m, 1H), 8.50-8.65 (d, *J* = 7.6 Hz, 1H), 11.84 (s, 1H), 13.00-14.00 (br s, 1H); ^{13}C NMR (100 MHz, DMSO-d_6) δ 45.1, 120.2, 120.4, 122.7, 123.2, 124.2, 125.7, 131.6, 132.3, 145.8, 148.2, 166.4, 167.6, 168.0, 197.3; LC-TOF (M+H$^+$) calcd for $C_{13}H_8FN_2O_4S_2$ 338.9910, found 338.9912.

(*Z*)-2-(5-(7-Chloro-2-oxoindolin-3-ylidene)-4-oxo-2-thioxothiazolidin-3-yl)acetic acid (**2037**). This compound was synthesized using general method A (75%): ^{1}H NMR (400 MHz, DMSO-d_6) δ 4.78 (s, 2H), 7.08-7.12 (dd, *J* = 8.0, 8.0 Hz, 1H), 7.49-7.51 (d, *J* = 8.0 Hz, 1H), 8.70-8.75 (d, *J* = 8.0 Hz, 1H), 11.72 (s, 1H), 13.00-14.00 (br s, 1H); ^{13}C NMR (100 MHz, DMSO-d_6) δ 45.1, 115.3, 121.8, 123.6, 125.8, 126.6, 131.7, 133.1, 142.6, 166.4, 167.5, 168.2, 197.3; LC-TOF (M+H$^+$) calcd for $C_{13}H_8ClN_2O_4S_2$ 354.9614, found 354.9619.

(*Z*)-2-(5-(5,7-Dichloro-2-oxoindolin-3-ylidene)-4-oxo-2-thioxothiazolidin-3-yl)acetic acid (**2039**). This compound was synthesized using general method A (71%): ^{1}H NMR (400 MHz, DMSO-d_6) δ 4.81 (s, 2H), 7.70 (s, 1H), 8.74 (s, 1H), 8.85 (s, 1H), 11.90 (s, 1H), 13.00-14.00 (br s, 1H); ^{13}C NMR (100 MHz, DMSO-d_6) δ 44.4, 115.7, 122.1, 124.3, 125.6, 131.6, 133.2, 141.3, 165.9, 166.3, 166.9, 167.2, 167.7, 194.6, 196.7; LC-TOF (M+H$^+$) calcd for $C_{13}H_7Cl_2N_2O_4S_2$ 388.9224, found 388.9224.

(*Z*)-2-(5-(5-Bromo-2-oxoindolin-3-ylidene)-4-oxo-2-thioxothiazolidin-3-yl)acetic acid (**2041**). This compound was synthesized using general method A (72%): ^{1}H NMR (400 MHz, DMSO-d_6) δ 4.77 (s, 2H), 6.87-6.89 (d, *J* = 8.0 Hz, 1H), 7.55-7.57 (d, *J* = 7.6 Hz, 1H), 8.85 (s, 1H), 11.40 (s, 1H), 13.00-14.00 (br s, 1H); ^{13}C NMR (100 MHz, DMSO-d_6) δ 45.2, 113.2, 114.2, 121.9, 125.3, 127.3, 130.2, 131.8, 135.8, 144.5, 166.8, 167.7, 167.9, 197.4; LC-TOF (M+H$^+$) calcd for $C_{13}H_8BrN_2O_4S_2$ 398.9109, found 398.9111.

Ethyl 2-(3-(4-oxo-2-thioxothiazolidin-3-yl)propanamido)acetate (**3019**). To a mixture of 3-(4-oxo-2-thioxothiazolidin-3-yl)propanoic acid (205 mg, 1.0 mmol), H_2N-Gly-OEt hydrochloride (140 mg, 1.0 mmol) and EDC (192 mg, 1.0 mmol) in DMF (5.0 mL) was

added triethylamine (140 µL, 1.0 mmol). The reaction mixture was stirred at room temperature for 16 h, and then concentrated. The crude product was purified by flash chromatogrphy (EtOAc/Hexanes 1:2-1:1) to give FX-3019 as a white solid (276 mg, 0.95 mmol, 95%): ^{1}H NMR (400 MHz, DMSO-d_6) δ 1.25-1.30 (t, J = 6.8 Hz, 3H), 2.64-2.70 (t, J = 7.6 Hz, 2H), 4.01 (s, 3H), 4.20-4.25 (dd, J = 7.2, 14.0 Hz, 2H), 4.25-4.35 (t, J = 8.0 Hz, 2H), 6.04 (s, 1H); ^{13}C NMR (100 MHz, DMSO-d_6) δ 14.1, 32.7, 35.4, 40.6, 41.4, 61.7, 169.4, 169.8, 173.6, 201.0; LC-TOF (M+H$^+$) calcd for $C_{10}H_{15}N_2O_4S_2$ 291.0473, found 291.0472.

(*Z*)-Ethyl-2-(3-(5-(5-chloro-2-oxoindolin-3-ylidene)-4-oxo-2-thioxothiazolidin-3-yl)propanamido) acetate (**3021**). This compound was synthesized using general method A (75%): ^{1}H NMR (400 MHz, DMSO-d_6) δ 1.15-1.20 (t, J = 7.2 Hz, 3H), 2.50-2.65 (t, J = 7.6 Hz, 2H), 3.76-3.80 (d, J = 5.6 Hz, 2H), 4.04-4.10 (dd, J = 6.8, 15.0 Hz, 2H), 4.20-4.30 (m, 2H), 6.97-7.00 (d, J = 7.6 Hz, 1H), 7.47-7.49 (d, J = 7.6 Hz, 1H), 8.50 (s, 1H), 8.83 (s, 1H), 11.41 (s, 1H); ^{13}C NMR (100 MHz, DMSO-d_6) δ 14.1, 31.7, 40.4, 40.7, 60.4, 112.2, 121.1, 123.7, 126.0, 127.0, 132.2, 133.0, 143.3, 166.7, 167.8, 169.6, 169.7, 197.1; LC-TOF (M+H$^+$) calcd for $C_{18}H_{17}ClN_3O_5S_2$ 454.0298, found 454.0437.

(*Z*)-3-(5-(5-Chloro-2-oxoindolin-3-ylidene)-2,4-dioxothiazolidin-3-yl)propanoic acid (**3039**). This compound was synthesized using general method A (71%): ^{1}H NMR (400 MHz, DMSO-d_6) δ 2.60-2.70 (t, J = 7.6 Hz, 2H), 3.80-3.90 (t, J = 7.6 Hz, 2H), 6.90-7.00 (d, J = 8.0 Hz, 1H), 7.40-7.50 (dd, J = 2.4, 8.0 Hz, 1H), 8.79-8.80 (d, J = 2.4 Hz, 1H), 11.37 (s, 1H), 12.42 (br s, 1H); ^{13}C NMR (100 MHz, DMSO-d_6) δ 31.4, 37.0, 112.0, 121.1, 125.9, 127.2, 132.0, 142.6, 165.4, 168.1, 169.5, 171.9; LC-TOF (M+H$^+$) calcd for $C_{14}H_{10}ClN_2O_5S$ 352.9999, found 353.0012.

3-(5-(5-Fluoro-3-hydroxy-2-oxoindolin-3-yl)-4-oxo-2-thioxothiazolidin-3-yl)propanoic acid (**2021**). This compound was synthesized using general method B (68%): ^{1}H NMR (400 MHz, DMSO-d_6) δ 1.70-1.80 (m, 1H), 2.06-2.14 (m, 3H), 3.70-3.80

(m, 1H), 3.86-3.93 (m, 1H), 6.80-6.90 (m, 1H), 7.10-7.20 (m, 1H), 10.70 (s, 1H), 12.50 (br s, 1H); ^{13}C NMR (100 MHz, CD_3OD) δ 29.6, 39.1, 57.7, 111.1, 111.2, 111.7, 111.9, 116.8, 117.0, 128.3, 138.4, 157.5, 159.9, 171.7, 172.1, 200.6. LC-TOF ($M+H^+$) calcd for $C_{14}H_{12}FN_2O_5S_2$ 371.0172, found 371.0166.

3-(5-(5-Chloro-3-hydroxy-2-oxoindolin-3-yl)-4-oxo-2-thioxothiazolidin-3-yl)propanoic acid (**2023**). This compound was synthesized using general method B (84%): ^{1}H NMR (400 MHz, DMSO-d_6) δ 1.60-1.70 (m, 1H), 2.00-2.10 (m, 1H), 3.70-3.80 (m, 1H), 3.86-3.94 (m, 1H), 5.10 (s, 1H), 6.85-6.87 (d, J = 8 Hz, 1H), 7.30 (s, 1H), 7.34-7.38(m, 2H), 10.8 (s, 1H), 12.5(br s, 1H); ^{13}C NMR (100 MHz, DMSO-d_6) δ 29.9, 38.9, 58.0, 75.1, 111.8, 124.0, 125.8, 128.9, 130.4, 141.5, 171.2, 171.5, 175.2, 201.0; LC-TOF ($M+H^+$) calcd for $C_{14}H_{12}ClN_2O_5S_2$ 386.9876, found 386.9865.

3-(5-(5-Bromo-3-hydroxy-2-oxoindolin-3-yl)-4-oxo-2-thioxothiazolidin-3-yl)propanoic acid (**2025**). This compound was synthesized using general method B (83%): ^{1}H NMR (400 MHz, DMSO-d_6) δ 1.60 (m, 1H), 2.10 (m, 1H), 3.70 (m, 1H), 3.9(m, 1H), 5.10 (s, 1H), 6.81-6.83 (d, J = 8 Hz, 1H), 7.30 (s, 1H), 7.40-7.50 (m, 2H), 10.90 (s, 1H), 12.50 (br s, 1H); ^{13}C NMR (100 MHz, DMSO-d_6) δ 30.2, 39.3, 58.5, 75.5, 112.7, 113.8, 127.1, 129.7, 133.7, 142.2, 171.5, 171.8, 175.5, 201.4; LC-TOF ($M+H^+$) calcd for $C_{14}H_{12}BrN_2O_5S_2$ 430.9371, found 430.9382.

3-(5-(3-Hydroxy-5-iodo-2-oxoindolin-3-yl)-4-oxo-2-thioxothiazolidin-3-yl)propanoic acid (**2027**). This compound was synthesized using general method B (81%): ^{1}H NMR (400 MHz, DMSO-d_6) δ 1.50-1.60 (m, 1H), 2.06-2.10 (m, 1H), 3.70-3.80 (m, 1H), 3.86-3.93 (m, 1H), 5.10 (s, 1H), 6.69-6.71 (d, J = 8 Hz, 1H), 7.3 (s, 1H), 7.61-7.64 (m, 2H), 10.80 (s, 1H), 12.5 (br s, 1H); ^{13}C NMR (100 MHz, DMSO-d_6) δ 30.2, 39.3, 58.6, 75.5, 85.0, 113.1, 129.9, 132.7, 139.4, 142.6, 171.6, 171.8, 175.3, 201.5; LC-TOF ($M+H^+$) calcd for $C_{14}H_{12}IN_2O_5S_2$ 478.9232, found 478.9236.

Kinase inhibition assay

For testing additional off-target effects that might result from unexpected activity against key enzyme therapeutic targets such as kinases we tested the effect of FX1 10 μM against a 50-kinase panel. The assay was performed at Nanosyn Inc (Santa Clara, CA), using purified recombinant kinase enzymes with concentrations of ATP at the apparent Km of each kinase, and FAM-labeled peptide substrates. The experiment was performed in duplicates and the kinase activity was measured by the change in electrophoretic mobility of the fluorescent-labeled substrate upon phosphorylation.

High-throughput RNA sequencing (RNAseq)

A total of 3 mg of total RNA was isolated from SUDHL-4, SUDHL-6, and Farage cells after 12 hr treatment with FX1 or vehicle. The RNAeasy Plus Kit (QIAGEN, Valencia, CA) that included a genomic DNA elimination step was used for RNA isolation. RNA concentration and purity were determined using Nanodrop (Life Technologies Corp., Grand Island, NY) and integrity was verified using Agilent 2100 Bioanalyzer (Agilent Technologies, Santa Clara, CA). Libraries were generated using an mRNA-seq sample prep kit (Illumina, San Diego, CA) according to manufacturer's instructions and then sequenced by Illumina HiSeq 2000 with single end 50-bp read length. The BCL6 siRNA RNAseq was as previously described (14). Raw image data were converted into base calls and fastq files via the Illumina pipeline CASAVA version 1.8 with default parameters. All 50-bp-long reads were mapped to the reference human genome sequence, hg19, using Tophat (version: tophat-2.0.14.Linux_x86_64) with the default parameters (15).(15). The mRNA expression levels for each gene (transcript) was represented as FPKM (fragments per kilobase of transcript per million fragments mapped) calculated by the Cufflinks package (version: cufflinks-2.2.1.Linux_x86_64, (15)).

Quantitative RT-PCR.

SUDHL-4 and SUDHL-6 cells were treated for 4, 8, 12, or 24 hours with 50 μM FX1, 79-6 or vehicle. Total RNA was extracted from drug treated and vehicle cells using RNeasy Plus kit (Qiagen, Valencia, CA) following the manufacturer instructions. cDNA was synthesized using the Verso cDNA synthesis kit (Life Technologies Corp., Grand Island, NY). We amplified specific genes with the following primers:

DUSP5: ATGGATCCCTGTGGAAGACA and TCACAGTGGACCAGGACCTT,

CXCR4: AGGCCCTAGCTTTCTTCCAC and CTGCTCACAGAGGTGAGTGC,

Caspase-8: CTGGGAGAAGGAAAGTTGGA and CAAGGCTGCTGCTTCTCTCT,

CDKN1A: CTGAAGGGTCCCCAGGTG and TAGGGCTTCCTCTTGGAGAA,

CD69: CTGGTCACCCATGGAAGTG and CATGCTGCTGACCTCTGTGT,

using the Fast SYBR Green conditions (initial step of 20 sec at 95 °C followed by 40 cycles of 1 sec at 95C and 20 sec at 60C). The CT values of the housekeeping gene (HPRT) were averaged and subtracted from the corresponding genes of interest (Δ^{CT}). The standard deviation of the difference was calculated from the standard deviation of the CT values (triplicates). Then, the Δ^{CT} values of the drug-treated cells were expressed relative to their respective vehicle-treated cells using the $\Delta\Delta^{CT}$ method. The fold change in expression for each gene in cells treated with the drug relative to vehicle treated cells is determined by the expression: $2\text{-}\Delta\Delta^{CT}$. Results were represented as the average fold change in expression with the standard error of the mean (SEM) for three sets of triplicates.

Chromatin immunoprecipitation (ChIP).

$3x10^7$ SUDHL-4 or SUDHL-6 cells were exposed to 50 μM FX1 or vehicle for 120 min. Cells were then fixed with 1% formaldehyde (Life Technologies Corp., Grand Island, NY)

for 10 minutes at room temperature. Cross-linking reaction was stopped by addition of 125mM glycine and cells were washed twice with cold PBS and lysed in lysis buffer (150mM NaCl, 1%v/v Nonidet P-40, 0.5% w/v deoxycholate, 0.1% w/v SDS, 50mM Tris pH8, 5mM EDTA, protease inhibitors). Cell lysates were sonicated using Covaris S220 AFA Ultrasonicator (Covaris Inc, Woburn, MA, USA) to generate fragments less than 400bp. Sonicated lysates were centrifuged, precleared with protein A beads (Roche Applied sciences, Manheim, Germany) and incubated overnight at 4^{o}C with specific BCL6 N-3 (Rabbit polyclonal Ab cat# sc-858 Santa Cruz Biotechnology, CA, USA), BCOR (Rabbit polyclonal antibody, kindly given by Dr. Vivian Bardwell, University of Minnesota, MN, USA), SMRT (Rabbit polyclonal Ab cat# 06-891 Millipore, MA, USA), or control IgG antibody (Rabbit polyclonal Ab cat# ab46540 Abcam, MA, USA). Immunocomplexes were recovered by adding 30ul protein A agarose beads (Roche Applied sciences, Manheim, Germany) for 1h at 4^{o}C rocking. Beads were sequentially washed twice with RIPA buffer, increasing stringency ChIP wash buffers at each step (150mM NaCl, 250mM NaCl, 250mM LiCl), and finally TE buffer. Immunocomplexes were eluted by adding elution buffer (1% SDS, 100mM $NaHCO_3$) and cross-linking was reverted by addition of 300mM NaCl and incubation at 65°C for at least 5h. DNA was purified using a PCR purification kit (Qiagen, Valencia, CA). A fraction of the ChIP product was used as template in 10ul real time PCR reactions using SYBR Green (PerfeCTa SYBR Green FastMix Reaction Mixes, Quanta Biosciences, Gaithesburg, MD) and 7900HT Fast Real-Time PCR System with 384-Well Block Module thermal cycler (Applied Biosystems, Manheim, Germany). Input chromatin standard curves were used for estimation of relative enrichment. Primer sequences were used as previously described in (14).

Germinal center formation

For analysis of the GCs formation, C57BL/6 mice (Jackson labs, Bar Harbor, ME, USA) were immunized intraperitoneally with sheep red blood cells (SRBC) (1×10^8 cells per mouse). Mice were treated intraperitoneally with 80 mg/kg/day FX1 or vehicle alone between 48 hours - 10 days after immunization.

Immunohistology: spleens were fixed in 4% paraformaldehyde (Life Technologies Corp., Grand Island, NY) and embedded in paraffin. 6 µm thick sections of each sample were prepared, cleared in xylene and hydrated through a descending alcohol series to distilled water. Slides were boiled for 20 minutes in citrate antigen retrieval buffer, followed by three washes with water. Endogenous peroxidase activity was blocked by treatment with 3% hydrogen peroxide in methanol. Tissue sections were then incubated overnight at 4 °C with biotin-conjugated peanut agglutinin (Vector Laboratories, Burlingame, CA), biotin-conjugated anti-B220 (Life Technologies Corp., Grand Island, NY, #RM2615), or Ki67 (Vector Laboratories, Burlingame, CA. #VP-K451). After a further wash in TBS, streptavidin–horseradish peroxidase was added, followed by incubation for 30 min. Horseradish peroxidase activity was detected with a DAB kit (Vector Laboratories, Burlingame, CA). Finally, sections were counterstained with hematoxylin if necessary.

Flow cytometric analysis: single-cell suspensions from mouse spleens were stained using the following fluorescent-labeled anti-mouse antibodies: PE-Cy7 conjugated anti-B220 (eBiosciences, San Diego, CA, #25-0452), PE-Cy7 conjugated anti-CD21 (Biolegend, San Diego, CA, # 123420) PE conjugated anti-CD23 (eBiosciences, San Diego, CA, #12-0232), APC conjugated anti-IgM (eBiosciences, San Diego, CA, #17-5790), APC conjugated anti-B220 (BD Biosciences, San Jose, CA, #553092), PE conjugated anti-FAS (BD Biosciences, San Jose, CA, #554258), FITC conjugated anti-GL7 (BD Biosciences, San Jose, CA, #553666), PE conjugated anti-IgD (BD Biosciences, San Jose, CA, #558597). DAPI was used for the exclusion of dead cells.

Data were acquired on MacsQuant flow cytometer (Miltenyi Biotec Inc., San Diego, CA) and analyzed using FlowJo software package (TreeStar, Ashland, OR).

Mice pharmacokinetic study.

Six to eight-week old male SCID mice were subcutaneously injected in the left flank with low-passage 10^7 human SUDHL-6 cells. When tumors reached 1000 mm3, mice were injected i.p. with 50 mg/kg of compound in vehicle (35% PEG-300, 5% Tween-80, 65% Dextrose 5%, n=8) or vehicle alone (n=2). Blood and tumors were harvested at different time points after injection (0 h, 0.5 h, 2 h, 4 h, 6 h, 8 h and 24 h). A gross necropsy was performed on all mice.

For quantitative HPLC analysis, blood samples were homogenized in EtOH:H_2O (2:1) solution at a 1:3 w/v ratio. The amounts of FX1 were determined by high-performance liquid chromatography-tandem mass spectrometry (HPLC-MS/MS) at the Department of Pharmaceutical Sciences, University of Maryland School of Pharmacy. Calibration curves were determined for the compound to convert the peak areas to compound concentration against the external reference standards. The tandem MS/MS detector also permits verification of peak identity as well as a quantitative assessment of the compounds in the samples. Results are expressed as µM of FX1 normalized to vehicle (time 0).

For QPCR, tumors were fast-frozen by immersion in liquid nitrogen and pulverized using the automated cryogenic sample pulverization system (CP02 Cryoprep Pulverizer, Covaris Inc. MA, USA). Total RNA was extracted using RNeasy Plus kit (Qiagen) following the manufacturer instructions. cDNA was synthesized using the Verso cDNA synthesis kit (Thermo).

We amplified specific genes with the following primers:

DUSP5: ATGGATCCCTGTGGAAGACA and TCACAGTGGACCAGGACCTT,

CXCR4: AGGCCCTAGCTTTCTTCCAC and CTGCTCACAGAGGTGAGTGC,

Caspase-8: CTGGGAGAAGGAAAGTTGGA and CAAGGCTGCTGCTTCTCTCT,

CDKN1A: CTGAAGGGTCCCCAGGTG and TAGGGCTTCCTCTTGGAGAA,

CD69: CTGGTCACCCATGGAAGTG and CATGCTGCTGACCTCTGTGT,

using the Fast SYBR Green conditions (initial step of 20 sec at 95C followed by 40 cycles of 1 sec at 95C and 20 sec at 60C). The CT values of the housekeeping gene (HPRT) were averaged and subtracted from the corresponding genes of interest (Δ^{CT}). The standard deviation of the difference was calculated from the standard deviation of the CT values (triplicates). Then, the Δ^{CT} values of the drug-treated cells were expressed relative to their respective vehicle-treated cells using the $\Delta\Delta^{CT}$ method. The fold change in expression for each gene in cells treated with the drug relative to vehicle treated cells is determined by the expression: $2\text{-}\Delta\Delta^{CT}$. Results were represented as the average fold change in expression with the standard error of the mean (SEM) for three sets of triplicates.

Mice toxicity studies

Six to eight-week old male C57BL/6 mice were purchased from the Jackson Labs (ME, USA) and housed in a barrier environment. Toxicity study 1: Five mice were exposed to daily intraperitoneal (IP) administration of increasing doses of FX1 ranging from 50 to 150 mg/kg in vehicle (35% PEG-300, 5% Tween-80, 65% Dextrose 5%) or vehicle alone (n=5) over the course of 10 days to a cumulative dose of 1125 mg/kg. Toxicity study 2: Five mice were exposed to daily IP administration of 100 mg/kg of FX1 in (35% PEG-300, 5% Tween-80, 65% Dextrose 5%) or vehicle alone (n=5) over the course of 10 days to a cumulative dose of 1000 mg/kg. In both studies, mice were examined and weighed every other day during the treatment period. At the moment of euthanasia, blood was collected and the organs were harvested and weighed. All organs and tissues

underwent extensive macroscopic and microscopic examination by veterinarian pathologists from the Research Animal Resource Center of Weill Medical College and by the author (R.S.). Microscopic examination included the following tissues: brain, heart, lungs, kidneys, liver, spleen, pancreas, intestines (small and large), bone marrow and skeletal muscle.

Western Blots

Western blot extracts were prepared by lysing $1x10^6$ cells in cold RIPA buffer in the presence of protease inhibitors (Sigma-Aldrich, St. Louis, MO). After centrifugation to remove cell debris, protein concentration was quantified using the Bradford protein assay kit (Thermo Fisher, Walthman, MA, USA). Normalized cell lysates were then mixed with sample buffer containing 2-mercaptoethanol and SDS and heated for 5 minutes at 95°C. Equal amounts of protein were run on SDS-polyacrylamide gels before being transferred to PVDF membranes. Binding of the primary antibodies against BCL6 (BCL6 D8 Mouse monoclonal Ab cat# sc-7388, Santa Cruz Biotechnology, CA, USA), and β-actin (Mouse monoclonal Ab Cat# A-5441, Sigma-Aldrich, St. Louis, MO) was detected with enhanced chemiluminescence reagent (Thermo Fisher, Walthman, MA, USA) using HRP-conjugated secondary antibody (Goat anti-mouse Ab cat# sc-2005, Santa Cruz Biotechnology, CA, USA).

BCL6 expression vectors, lentivirus production and infection

cDNA fragments encoding BCL6 were sub-cloned into pcDH-EF-T2A puromycin Lentivirus expression vector (System Biosciences, Mountain View, CA). Viral production and concentration were followed according to the standard protocol. Lymphoma cells were infected with concentrated virus in the presence of 8μg/ml polybrene (Sigma-Aldrich, st. Louis, MO). Five days after infection, puromycin-resistant cells were selected

by adding 2 μg/ml puromycin (Life Technologies Corp., Grand Island, NY) as previously described (16).

ABC- GCB-DLBLC classification based on gene expression profile

We adapted the method published in Wright et al. (17) to classify DLBCL samples into ABC- and GCB-DLBCL subtypes. We use the microarray dataset from Rosenwald et al. (18) as training data, which has pre-determined ABC/GCB classification labels. With the goal of being able to classify datasets from different platforms, we first apply rank normalization to both training and the to-be-classified data, where for each gene the rank of expression level across all samples is used instead of raw expression level. Then we select the top 100 most differentially expressed genes ranked by p value between the ABC and GCB groups in the training data as determined by student's t-test as genes in the Bayesian predictor. A linear predictor score (LPS) for each sample in the training and to-be-classified data is then calculated,

$$LPS(X) = \sum_{j=1}^{100} a_j X_j$$

where X_j is the expression level of j th gene in the predictor and a_j is the t statistic of j th gene in the t test. Then we calculate the likelihood that a sample is in each of the two subgroups by applying Bayes' rule:

$$P(X\ in\ group\ 1) = \frac{\phi(\mathrm{LPS(X)}; \hat{\mu}_1, \hat{\sigma}_1^2)}{\phi(\mathrm{LPS(X)}; \hat{\mu}_1, \hat{\sigma}_1^2) + \phi(\mathrm{LPS(X)}; \hat{\mu}_2, \hat{\sigma}_2^2)}$$

where $\phi(\mathrm{LPS(X)}; \hat{\mu}, \hat{\sigma}^2)$ represents the normal density function given mean $\hat{\mu}$ and variance $\hat{\sigma}^2$ estimated from a training set subgroup. We set 90% certainty as cutoff for subgroup assignment.

Supplemental Bibliography

1. Guvench O, and MacKerell AD, Jr. Computational fragment-based binding site identification by ligand competitive saturation. *PLoS Comput Biol.* 2009;5(7):e1000435.
2. Raman EP, Yu W, Guvench O, and Mackerell AD. Reproducing crystal binding modes of ligand functional groups using Site-Identification by Ligand Competitive Saturation (SILCS) simulations. *Journal of chemical information and modeling.* 2011;51(4):877-96.
3. Raman EP, Yu W, Lakkaraju SK, and MacKerell AD, Jr. Inclusion of multiple fragment types in the site identification by ligand competitive saturation (SILCS) approach. *Journal of chemical information and modeling.* 2013;53(12):3384-98.
4. Yu W, Lakkaraju SK, Raman EP, Fang L, and MacKerell AD, Jr. Pharmacophore modeling using site-identification by ligand competitive saturation (SILCS) with multiple probe molecules. *Journal of chemical information and modeling.* 2015;55(2):407-20.
5. Ahmad KF, Melnick A, Lax S, Bouchard D, Liu J, Kiang CL, Mayer S, Takahashi S, Licht JD, and Prive GG. Mechanism of SMRT corepressor recruitment by the BCL6 BTB domain. *Molecular cell.* 2003;12(6):1551-64.
6. Word JM, Lovell SC, Richardson JS, and Richardson DC. Asparagine and glutamine: using hydrogen atom contacts in the choice of side-chain amide orientation. *J Mol Biol.* 1999;285(4):1735-47.
7. Hess B. GROMACS 4: Algorithms for Highly Efficient, Load-Balanced, and Scalable Molecular Simulation. *J Chem Theory Comput.* 2008;4 (3):435–47.
8. MacKerell AD, Bashford D, Bellott M, Dunbrack RL, Evanseck JD, Field MJ, Fischer S, Gao J, Guo H, Ha S, et al. All-atom empirical potential for molecular modeling and dynamics studies of proteins. *J Phys Chem B.* 1998;102(18):3586-616.
9. Best RB, Zhu X, Shim J, Lopes PE, Mittal J, Feig M, and Mackerell AD, Jr. Optimization of the additive CHARMM all-atom protein force field targeting improved sampling of the backbone phi, psi and side-chain chi(1) and chi(2) dihedral angles. *J Chem Theory Comput.* 2012;8(9):3257-73.
10. Vanommeslaeghe K, Hatcher E, Acharya C, Kundu S, Zhong S, Shim J, Darian E, Guvench O, Lopes P, Vorobyov I, et al. CHARMM general force field: A force field for drug-like molecules compatible with the CHARMM all-atom additive biological force fields. *J Comput Chem.* 2010;31(4):671-90.
11. Vanommeslaeghe K, and MacKerell AD, Jr. Automation of the CHARMM General Force Field (CGenFF) I: bond perception and atom typing. *Journal of chemical information and modeling.* 2012;52(12):3144-54.
12. Vanommeslaeghe K, Raman EP, and MacKerell AD, Jr. Automation of the CHARMM General Force Field (CGenFF) II: assignment of bonded parameters and partial atomic charges. *Journal of chemical information and modeling.* 2012;52(12):3155-68.
13. William L. Jorgensen JDM. Quantum and statistical mechanical studies of liquids. 25. Solvation and conformation of methanol in water. *J Am Chem Soc.* 1983;105 (6):1407–13.
14. Hatzi K, Jiang Y, Huang C, Garrett-Bakelman F, Gearhart MD, Giannopoulou EG, Zumbo P, Kirouac K, Bhaskara S, Polo JM, et al. A hybrid mechanism of action for BCL6 in B cells defined by formation of functionally distinct complexes at enhancers and promoters. *Cell reports.* 2013;4(3):578-88.

15. Trapnell C, Roberts A, Goff L, Pertea G, Kim D, Kelley DR, Pimentel H, Salzberg SL, Rinn JL, and Pachter L. Differential gene and transcript expression analysis of RNA-seq experiments with TopHat and Cufflinks. *Nat Protoc.* 2012;7(3):562-78.
16. Huang C, Geng H, Boss I, Wang L, and Melnick A. Cooperative transcriptional repression by BCL6 and BACH2 in germinal center B-cell differentiation. *Blood.* 2014;123(7):1012-20.
17. Wright G, Tan B, Rosenwald A, Hurt EH, Wiestner A, and Staudt LM. A gene expression-based method to diagnose clinically distinct subgroups of diffuse large B cell lymphoma. *Proceedings of the National Academy of Sciences of the United States of America.* 2003;100(17):9991-6.
18. Rosenwald A, Wright G, Chan WC, Connors JM, Campo E, Fisher RI, Gascoyne RD, Muller-Hermelink HK, Smeland EB, Giltnane JM, et al. The use of molecular profiling to predict survival after chemotherapy for diffuse large-B-cell lymphoma. *The New England journal of medicine.* 2002;346(25):1937-47.

Supplemental Tables

Therapeutic Targeting of GCB- and ABC-DLBCLs by Rationally Designed BCL6 Inhibitors

Mariano G Cardenas[1], Wenbo Yu[2#], Wendy Beguelin[1], Matthew R Teater[1], Huimin Geng[1, 3], Rebecca L. Goldstein[1], Erin Oswald[1], Katerina Hatzi[1], Shao-Ning Yang[1], Joanna Cohen[1], Rita Shaknovich[1], Kenno Vanommeslaeghe[2], Huimin Cheng[2], Dongdong Liang[2], Hyo Je Cho[4], Joshua Abbott[4], Wayne Tam[5], Wei Du[6], John P. Leonard[1], Olivier Elemento[6], Leandro Cerchietti[1*], Tomasz Cierpicki[4*], Fengtian Xue[2*], Alexander D. MacKerell, Jr.[2*], Ari M. Melnick[1*].

[1]Weill Cornell Medical College, Department of Hematology/Oncology, New York, NY. [2]Computer-Aided Drug Design Center, University of Maryland, School of Pharmacy, Department of Pharmaceutical Sciences, Baltimore, MD. [3]University of California San Francisco, Department of Laboratory Medicine, San Francisco, CA, USA. [4]University of Michigan, Department of Pathology, Ann Arbor, MI. [5]Department of Pathology and Laboratory Medicine, Weill Cornell Medical College, NY, USA. [6]Department of Physiology and Biophysics, Weill Cornell Medical College, NY, USA. [#]Considered co-first author. [*]Corresponding authors.

Table1. Kinase panel used to test FX1 off-target effects.

Name	Symbol	Full name
ABL1	ABL1	c-abl oncogene 1, non-receptor tyrosine kinase
AMP-A1B1G1	PRKAA1	protein kinase, AMP-activated, alpha 1 catalytic subunit
AURORA-A	AURKA	aurora kinase A
CAMK4	CAMK	calcium/calmodulin-dependent protein kinase IV
CDK1-CYCLINB	CDK1	cyclin-dependent kinase 1 / cyclinB
CDK2-CYCLINA	CDK2	cyclin-dependent kinase 2 / cyclinA
CHEK1	CHEK1	CHK1 checkpoint human homolog (S. pombe)
CK1-EPSILON	CSNK1E	casein kinase 1, epsilon
CSK	CSK	c-src tyrosine kinase
DAPK1	DAPK1	death-associated protein kinase 1
DYRK1A	DYRK1A	dual-specificity tyrosine-(Y)-phosphorylation regulated kinase 1A
EGFR	EGFR	epidermal growth factor receptor
EPH-A2	EPHA2	EPH receptor A2
FAK	PTK2	PTK2 protein tyrosine kinase 2
FGFR1	FGFR1	fibroblast growth factor receptor 1
FLT3	FLT3	fms-related tyrosine kinase 3
GSK3-BETA	GSK3B	glycogen synthase kinase 3 beta
IGF1R	IGF1R	insulin-like growth factor 1 receptor
IKK-BETA	IKBKB	inhibitor of kappa light polypeptide gene enhancer in B-cells, kinase beta
IRAK4	IRAK4	interleukin-1 receptor-associated kinase 4
ITK	ITK	IL2-inducible T-cell kinase
JAK1	JAK1	Janus kinase 1
JAK2	JAK2	Janus kinase 2
JNK2	MAPK9	mitogen-activated protein kinase 9
KDR	KDR	kinase insert domain receptor (a type III receptor tyrosine kinase)
LCK	LCK	lymphocyte-specific protein tyrosine kinase
MAP4K4	MAP4K4	mitogen-activated protein kinase kinase kinase kinase 4
MAPK1	MAPK1	mitogen-activated protein kinase 1
MAPKAPK2	MAPKAPK2	mitogen-activated protein kinase-activated protein kinase 2
MEK1	MAP2K1	mitogen-activated protein kinase kinase 1
MEK2	MAP2K2	mitogen-activated protein kinase kinase 2
MET	MET	met proto-oncogene (hepatocyte growth factor receptor)
MST1	STK4	serine/threonine kinase 4
MST2	STK3	serine/threonine kinase 3
NEK2	NEK2	NIMA (never in mitosis gene a)-related kinase 2
P38-ALPHA	MAPK14	mitogen-activated protein kinase 14
PAK2	PAK2	p21 protein (Cdc42/Rac)-activated kinase 2
PDGFR-ALPHA	PDGFRA	platelet-derived growth factor receptor, alpha polypeptide
PDK1	PDK1	pyruvate dehydrogenase kinase, isozyme 1
PI3K-ALPHA	PIK3CA	phosphoinositide-3-kinase, catalytic, alpha polypeptide
PIM1	PIM1	pim-1 oncogene
PKC-ALPHA	PRKCA	protein kinase C, alpha
PKA	PRKACA	protein kinase, cAMP-dependent, catalytic, alpha
PRKD2	PRKD2	protein kinase D2
PYK2	PTK2B	PTK2B protein tyrosine kinase 2 beta
ROCK1	ROCK1	Rho-associated, coiled-coil containing protein kinase 1
SGK1	SGK1	serum/glucocorticoid regulated kinase 1
SRC	SRC	v-src sarcoma (Schmidt-Ruppin A-2) viral oncogene homolog
SYK	SYK	spleen tyrosine kinase
TYK2	TYK2	tyrosine kinase 2

Table 2. Biochemistry parameters and complete blood counts from C57BL/6 mice treated with daily doses of FX1 100 mg/kg.

	Condition			
Parameter	Vehicle	FX1 100 mg/kg	Reference	Units
ALP	50	25	23-181	UI/L
ALT	24	25	16-58	UI/L
AST	133	168.75	36-102	UI/L
GGT	0	0	0-2	UI/L
ALBUMIN	3.5	3	2.5-3.9	g/dl
TOTAL PROTEIN	6	5.175	4.1-6.4	g/dl
GLOBULIN	2.5	2.5	1.3-2.8	g/dl
TOTAL BILIRUBIN	< 0.3	< 0.3	0-0.3	mg/dl
BUN	21.5	12	14-32	mg/dl
CREATININE	< 0.3	< 0.3	0.1-0.6	mg/dl
CHOLESTEROL	105.5	106.75	74-190	mg/dl
GLUCOSE	146	102.25	76-222	mg/dl
WBC	5.912	11.232	5.4-16	K/uL
RBC	8.786	9.344	6.7-9.7	M/uL
Hemoglobin	12.66	12.5	10.2-16.6	g/dL
Hematocrit	49.32	49.88	32-54	(%)
Platelets	410.6	785	799-1300	K/uL

Supplemental Table 3 - Characteristics of the patient samples used

Patient number	Age and gender	Site	Diagnostic	Hans Classification	Expression Classification	Immunohistochemistry					FISH			cytogenetics
						BCL6	CD10	MUM1	MYC	BCL2	MYC	BCL2	BCL6	NA
#1	50 F	left inguinal lymph node	DLBCL	non-GCB	Unclassified	POS	NEG	POS	NA	POS	NEG	NEG	NEG	47,XX,+X[3]/47~48,idem,add(4)(q3?3),+mar[cp16]
#2	70 F	spleen	DBLCL	non-GCB	GCB-DLBCL	POS	NEG	POS	NA	POS	NA	NA	NA	NA
#3	59 M	right axillary lymph node	DLBCL	non-GCB	ABC-DLBCL	POS	NEG	POS	NA	POS	NA	NA	POS rearranged	47,XY,t(3;22)(q27;q11.2),t(4;12)(q12;p11.2),add(8)(p11.2),add(8)(q11.2),-13,del(17)(q24),+18,+mar[19]/46,XY[2]